COMETARY SCIENCE

The landing(s) of Philae and inferences about comet surface mechanical properties

Jens Biele,[1]* Stephan Ulamec,[1] Michael Maibaum,[1] Reinhard Roll,[3] Lars Witte,[2] Eric Jurado,[9] Pablo Muñoz,[5,12] Walter Arnold,[10] Hans-Ulrich Auster,[6] Carlos Casas,[5,12] Claudia Faber,[4] Cinzia Fantinati,[1] Felix Finke,[1] Hans-Herbert Fischer,[1] Koen Geurts,[1] Carsten Güttler,[3] Philip Heinisch,[6] Alain Herique,[8] Stubbe Hviid,[4] Günter Kargl,[7] Martin Knapmeyer,[4] Jörg Knollenberg,[4] Wlodek Kofman,[8] Norbert Kömle,[7] Ekkehard Kührt,[4] Valentina Lommatsch,[1] Stefano Mottola,[4] Ramon Pardo de Santayana,[5,12] Emile Remetean,[9] Frank Scholten,[4] Klaus J. Seidensticker,[4] Holger Sierks,[3] Tilman Spohn[4]

The Philae lander, part of the Rosetta mission to investigate comet 67P/Churyumov-Gerasimenko, was delivered to the cometary surface in November 2014. Here we report the precise circumstances of the multiple landings of Philae, including the bouncing trajectory and rebound parameters, based on engineering data in conjunction with operational instrument data. These data also provide information on the mechanical properties (strength and layering) of the comet surface. The first touchdown site, Agilkia, appears to have a granular soft surface (with a compressive strength of 1 kilopascal) at least ~20 cm thick, possibly on top of a more rigid layer. The final landing site, Abydos, has a hard surface.

To land on comet 67P/ Churyumov-Gerasimenko (67P), Philae was ejected from the Rosetta main spacecraft with a predefined velocity, stabilized by a flywheel, and descended ballistically to the cometary surface. At touchdown it was planned to activate a cold gas system, pushing the lander to the surface, as well as firing two anchoring harpoons to fix Philae to the ground. Unfortunately, both subsystems did not work, leading to a bouncing of the lander. An analysis of the exact bouncing dynamics, however, fortuitously allowed determinations of the comet surface properties at the ~10-cm–to–meter scale.

The mechanical strength of cometary surface material cannot be measured remotely, yet it is an important parameter for understanding the evolution and activity of cometary nuclei. Furthermore, mechanical strength is linked to porosity and grain properties (*1*), thus providing insight into the structural features of cometary matter (*2*) and informing future comet missions. Indirect observations (*3*–*6*) and models (*2*, *3*) have resulted in wide ranges of material strength. The Deep Impact experiment on comet Tempel-1 yielded initially an extremely low ("effective") strength (<65 Pa) (*7*), raising questions as to whether a comet lander could land on such weak material. Experimental work on the aerodynamic (i.e., tensile?) strength of meteoroids (*5*), as well as particles collected by Stardust in the coma of comet 81P/Wild 2 (*6*), also indicated a strength range of 3 to 80 kPa on the submillimeter-to-centimeter scale. The landings of Philae, despite not proceeding as planned, provide direct observations of the surface mechanical properties and thus a baseline for comparison with these previous studies.

[1]Deutsches Zentrum für Luft- und Raumfahrt (DLR)/ Raumflugbetrieb und Astronautentraining, Microgravity User Support Center (MUSC), Linder Höhe 1, 51147 Cologne, Germany. [2]DLR/Institut für Raumfahrtsysteme, Robert Hooke-Straße 7, 28359 Bremen, Germany. [3]Max-Planck-Institut für Sonnensystemforschung (MPS), Justus-von-Liebig-Weg 3, 37077 Göttingen, Germany. [4]DLR/Institut für Planetenforschung Rutherfordstraße 2, 12489 Berlin, Germany. [5]European Space Agency/European Space Operations Centre (ESA/ESOC), Robert-Bosch-Straße 5, 64293 Darmstadt, Germany. [6]Institut für Geophysik und Extraterrestrische Physik, Technische Universität Braunschweig Mendelssohnstrasse 3, 38106 Braunschweig, Germany. [7]Institut für Weltraumforschung (IWF) Graz, Austria Austrian Academy of Sciences, Space Research Institute, Schmiedlstraße 6, 8042 Graz, Austria. [8]Université Grenoble Alpes and CNRS, Institut de Planétologie et d'Astrophysique de Grenoble, F-38000 Grenoble, France. [9]Centre National d'Études Spatiales, 18 Avenue Édouard Belin, 31400 Toulouse, France. [10]1. Physikalisches Institut, Georg August Universität, 37077 Göttingen, Germany; permanent address: Department of Materials Science, Saarland University, 66123 Saarbrücken, Germany. [11]Magellium, 24 Rue Hermès, Boîte Postale 12113, 31521 Ramonville Saint-Agne Cedex, France. [12]Grupo Mecánica de Vuelo at ESA/ESOC - GMV Robert-Bosch-Straße 5, 64293 Darmstadt, Germany.
***Corresponding author. E-mail: jens.biele@dlr.de**

Circumstances of Philae landings and bounces

On 12 November 2014, at 06:01 (all times are in UTC), a pre-delivery spacecraft maneuver put Rosetta in a hyperbolic trajectory with a 5-km miss distance to the comet nucleus, almost on a collision course with the comet. The distance from the Sun was 2.99 astronomical units (AU). At 07:20, Rosetta slewed to separation attitude. The (formal reconstructed 1σ) uncertainties in attitude, position, and velocity of the spacecraft with respect to the comet at separation were 0.015°, 10 m, and 2 mm/s, respectively. Separation occurred with a relative velocity (Δv) of 0.1876 m/s by the motor-driven mechanical separation device from the Rosetta orbiter at an altitude of about 20.5 km (radius vector = 22.7 km) and as planned on 12 November 2014, 08:35:00.

After 6:59:04 hours of ballistic descent, of which the first 90% were tracked by the CONSERT (Comet Nucleus Sounding Experiment by Radiowave Transmission) instrument (*8*, *9*), Philae landed at 15:34:03.98 ± 0.10 s, in Agilkia (formerly called "area J") on 67P. This instant (TD1, the first touchdown site) refers to the time of the trigger signal at the vertical axis of the +Y foot SESAME-CASSE (Surface Electrical Sounding and Acoustic Monitoring Experiments/Cometary Acoustic Sounding Surface Experiment) accelerometer (Fig. 1).

The design of the descent trajectory was such that the incoming velocity, in the comet-fixed frame, was at touchdown parallel to the normal of the target landing site. The descent reconstruction shows that the angle between the incoming velocity vector and the normal to the target landing site was 0.9°. The reconstructed landing site's local normal was 12° (slope) away from the target normal, and the incoming velocity was 11.5° away from the local normal at touchdown. The comet-fixed coordinates of the TD1 point are 112 m and only 51 s away from the targeted landing site and time (Table 1). A priori landing uncertainties were stated as ±500 m in position and ±40 min in time. The touchdown speed relative to the comet surface was about 1.0 m/s.

At touchdown, as foreseen, the central damping tube of Philae's landing gear was pushed in. The landing gear was designed such as to dissipate a large fraction of the lander impact kinetic energy by a damping motor within this mechanism. The damping coefficient was 567 Ns/m (*10*). The motion of the damping tube also generated the touchdown signal, which actually occurred at 15:34:06.471 ± 1 s. The stroke length of the damper was 42.6 ± 0.1 mm out of a full length of ~170 mm. During TD1, the lander tilt changed by −1.375° and +0.575° in two perpendicular axes and +0.335° in rotation around the z axis. The landing gear damper did not move after TD1; i.e., the component of force in the lander z direction during the further touchdowns must have been <30 N, due to static friction in the mechanism.

The signals recorded by the CASSE accelerometer mounted on the +Y foot, together with the translational motion of the damper, are shown in Fig. 1. Vibrations due to the flywheel as well as the noise of the recording system are below the least significant bit of the recording. There is an interval of 266 ms from the first samples that are different from zero until the beginning of the strong signal. The damper then takes another 170 ms until it clearly moves and another 250 ms until damping sets in. The damper motion in the following 156 ms was only recorded by the platform (end position), because the TD signal had been generated by then. Ultimately, the damping tube position moved from 199.6 to 156.9 mm.

Because the anchor harpoons did not fire upon touchdown and the hold-down thrust of the cold gas system did not work, the lander bounced several times until it came to rest after about

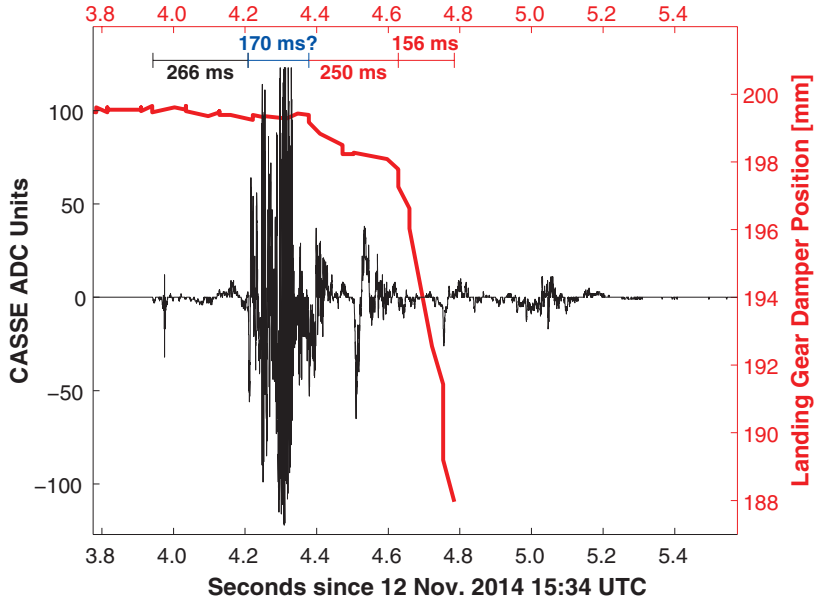

Fig. 1. Touchdown signals at Agilkia. Black: Vertical acceleration of the +Y foot as recorded by CASSE (sampling frequency of 5 kHz, 8-bit amplitude resolution; electronics include a high-pass filter, cutting off DC and frequencies below ~1 Hz). Peak accelerations were clipped. Red: Position of the damper as recorded by a potentiometer at intervals between 10 and 100 ms, terminating when position 188 mm was reached. The durations of the time intervals discussed in the text are indicated (black, based on CASSE data alone; red, based on landing gear data alone; blue, combined data with a higher systematic uncertainty).

Table 1. Main events of Philae's landings. ROMAP times (*17*) and MUPUS events and times (*12*). RMOC is ESA's Rosetta Mission Operation Centre at ESOC Darmstadt. Coordinates are comet-fixed and in the ESA-RMOC reference frame (version 00085).

Event	Onboard time 2014-11-12	Main source	Comments; coordinates where applicable ([*x*,*y*,*z*], unit km)
Separation from Rosetta	08:35:00 ± 1s	ESA flight dynamics	[−17.1652762547, 10.1582193407, 10.6887254384], 22.38 km radius
TD1 (Agilkia)	15:34:03.98 ± 0.10s	SESAME; Damper event time: 15:34:06.471	[2.123468, −0.959272, 0.497006] or 335.689° longitude, 12.041° latitude, 2.3825 km radius; see also table S2
COL (collision with crater rim)	16:20:00 ± 2s	Solar generator, MUPUS, ROMAP	For coordinates, see table S3
TD2	17:25:26 ± 1s	ROMAP, MUPUS	For coordinates, see table S3
TD3 (final rest, Abydos)	17:31:17 ± 1s	ROMAP	Most likely position: longitude 358.2°, latitude −8.2° (RMOC 00085 frame)
LOS (loss of signal)	17:59:44 ± 1 s	ESA flight dynamics	Final lander attitude determined by ROMAP, ffl15° uncertainties in all axes (*12*)

2 hours of ballistic flight. The S-band communications link was functional until 17:59:44 (an expected loss of signal due to orbiter-lander geometry), although numerous very short link breaks occurred roughly every 0.5 to 3.5 min, causing, however, almost no data loss. Unfortunately, the initial anchoring was not successful. This affected lander operations, in particular drilling, but in addition, the accelerometers connected with the harpoons could not carry out the various planned measurements as a function of depth (*11*).

After the TD1, the lander bounced. This soon became clear at the Lander Control Center (LCC, Cologne) when data from the solar generator was interpreted, indicating that the lander was rotating. Communications telemetry and the MUPUS TM (Multipurpose Sensors for Surface and Sub-Surface Science Thermal Mapper) and ROMAP (Rosetta Magnetometer and Plasma Monitor) instruments also indicated movement. Only after about 1:57 hours, at 17:31:17 (Table 1), Philae came to rest after having reached its final landing site.

About 27 min after the final landing, the communications link with the orbiter was interrupted for geometrical reasons. It was reestablished four more times, until the batteries ran out of power, early on 15 November. Visibility periods followed more or less the expected sequence; however, they were shorter than predicted for site Agilkia, and numerous brief link breaks were observed. The unexpected situation after landing (no anchoring and short illumination periods) led to the adaptation of the originally planned first scientific sequence (FSS), but eventually, all scientific instruments were activated. Because the exact location of Philae was unclear, three additional campaigns were executed, using CONSERT for ranging. Consequently, Philae's location was narrowed down to an area of 150 × 15 m^2, not taking into account the shape model uncertainties. New communication with Philae starting in June 2015, as well as very close approaches of Rosetta in the extended mission phase, will hopefully help refine the attitude and location estimates.

On 15 November 2014 00:07, the lander bus voltage dropped below 21 V, the threshold for lander platform operations, and the link between orbiter and lander broke. The battery lifetime was as expected. Philae entered "hibernation" (*12*). Table 1 gives an overview of the main events during Philae's landings.

We refer to the event at ~16:20 as a collision, not a touchdown, because no vertical deceleration of the ROMAP boom was detected. After this encounter, Philae started to tumble. The collision at about 16:20 must have been a very slight grazing contact, because it only changed the rotational characteristics measured clearly by ROMAP and MUPUS. It induced a stronger nutation and deflected the flight trajectory, but it did not lead to a crash or complete destabilization of the lander attitude.

Lander trajectory reconstruction

The bouncing trajectory could be constrained by optical images of the lander in flight, its shadow, and its end point by CONSERT ranging data, together with solar generator housekeeping (SG HK) values [mainly day length; see definition in (*12*)]. The times of touchdowns and collisions were derived from the analysis of SG HK, ROMAP, MUPUS, and SESAME data.

Two teams independently reconstructed the descent and bouncing trajectory of Philae: RMOC (Rosetta Mission Operations Centre, Flight Dynamics) and SONC (the Lander Science Operations and Navigations Centre) (*12*) (Figs. 2 and 3). The two reconstructions are based on similar sets of data but used slightly different comet models and constraints. They are very similar from the separation to the "collision," then diverge somewhat, but end in the same region. The differences after the collision are mainly due to the different sets of data used: The ESOC (European Space Operations Centre) reconstruction used observations of the lander in the OSIRIS (Optical, Spectroscopic, and Infrared Remote Imaging System) wide-angle camera (WAC) images at 16:45 and 17:20, with the end point of the trajectory as a free

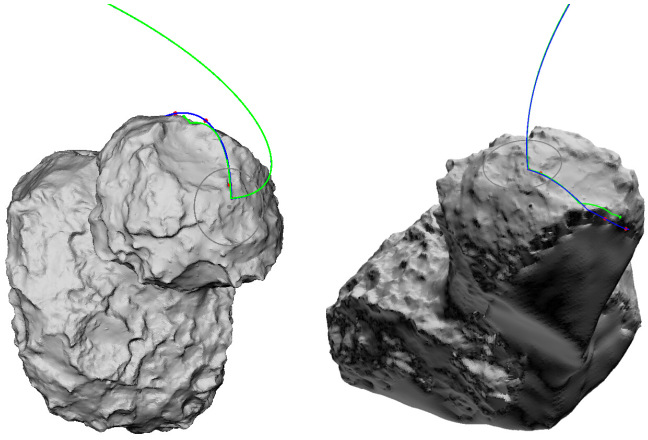

Fig. 2. SONC (green) and ESOC (blue) reconstructed trajectories in the comet-fixed frame from two observation angles (left and right panels). Plotting a three-dimensional trajectory in the rotating frame may give the impression that the collision at 16:20 has deflected the trajectory considerably, whereas in reality, the comet has rotated (29°/hour) as well. If the WAC observations (red dots) were indeed the lander, then the trajectory would be clearly higher, as indicated by ESOC reconstruction. Before the collision, the two reconstructions are very close. The SONC trajectory includes a third touchdown, which, however, is unconstrained except for its time. The shape model used for this figure was RMOC version 5.

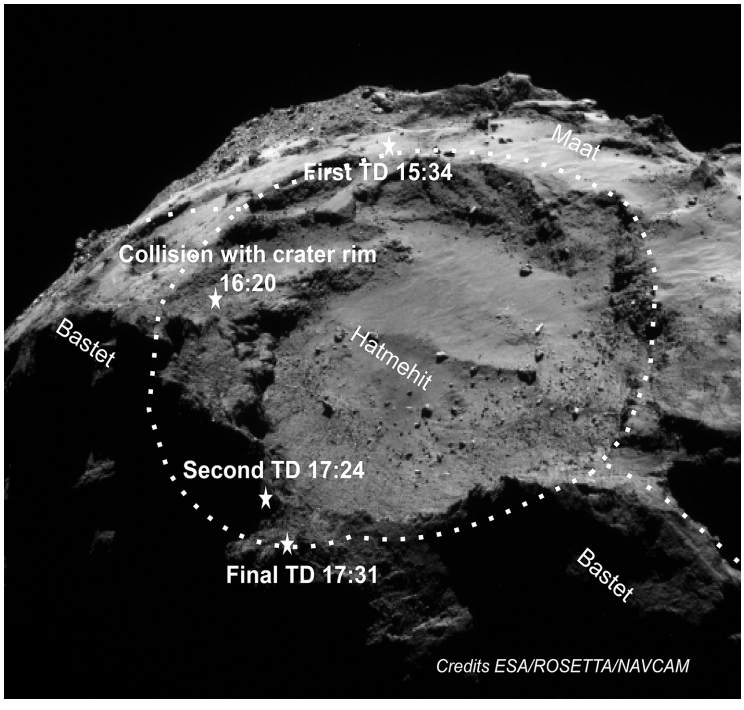

Fig. 3. Landing points (SONC) on a NAVCAM image. A second TD2, here taken at 17:24 (observed time: 17:25:26), is not modeled by RMOC and here only an example is given, because it is not well constrained. We expect that the last bounce was only a few meters.

parameter, whereas SONC reconstruction did not use these observations but constrained the end point of the trajectory to match the best estimate of the final landing site coordinates based on CONSERT measurements. Given the uncertainties of the near-surface gravity field (*12*) and the few observations in the last part of the trajectory, the agreement between these preliminary trajectories is quite satisfactory.

The reconstructed comet-fixed incoming velocity at TD1/rebound is, in the horizontal frame local to the landing point [east, north, up] (*12*) [2.0, −20.7, −99.0] cm/s, 101.2 cm/s in magnitude, 20.8 cm/s of lateral velocity; whereas outgoing conditions were [21.3, −23.5, 7.2] cm/s, 32.5 cm/s in magnitude, 31.7 cm/s of lateral velocity.

The pre-touchdown velocity component perpendicular to the surface was strongly reduced, whereas the north-south component was hardly affected. Most of the remaining kinetic energy went into a strong east-west lateral component, leading to a bouncing angle of 86.3 ± 0.5°. The escape velocity at Agilkia is ~0.9 m/s, slightly below the pre-touchdown velocity.

OSIRIS NAC (Narrow Angle Camera) images were used together with ROLIS (Rosetta Lander Imaging System) descent images for determining the actual landing coordinates and attitude at Philae's first landing site, Agilkia (Fig. 4 and Table 1). Altitude, attitude with respect to the surface, and the rotational state were derived independently from this analysis.

Philae has not yet been found unambiguously in optical images, so its final landing site Abydos is the area constrained by the CONSERT ranging data (*8*, *12*–*14*). It is consistent with the measured solar generator HK values (day length, sunrise, and sunset by solar cell output from the scattered light of the surroundings) and the new communications pattern starting on 13 June 2015 and telemetry received since then. Fortunately, this area in the Bastet (*15*) region is still near the equator and was imaged by the orbiter's cameras. A global and local digital terrain model with an effective resolution on the order of 5 to 10 m exists (*16*).

Description of the rebounds

After TD1, the lander retained its inertial z-axis attitude, but rotated much faster. ROMAP data (*17*) show to ~1-s accuracy when the lander touched the comet surface, revealing a triple bounce, touching the surface at the rim of the Hatmehit depression about 46 min after TD1. Eight seconds after TD1, the CASSE sensors were again in "listening mode" until 16:02:16 but registered no signal above the trigger limit of about 20 m/s^2.

OSIRIS and NAVCAM images have been used for reconstructing the trajectory. One of the images even shows the "footprints" at TD1, and another image shows the dust cloud produced by the impact (fig. S17). The rotation and attitude of Philae could be inferred from a number of observations, including ROMAP magnetometer data (*17*), solar generator HK values, MUPUS-TM sensor and thermal reference sensor data (*12*), and system temperature sensors. During descent, the rotation and attitude were also measured by CONSERT signal amplitude periodicities, by direct imaging by OSIRIS, and by analysis of ROLIS descent images. Directly after separation, the rotation period was 5.1 min (*17*). After the successful deployment of the landing gear, Philae's spin period changed to 8 to 10 min (~0.002 Hz), all counterclockwise (as seen from the top) around the lander z axis. This rotation was expected and is due to residual imperfections of the MSS and the change in the moments of inertia. The flywheel, which stabilized the lander in the z direction during descent, was switched off at TD1 and then ran down in ~32 min, transferring its angular momentum of 5.17 N·m/s by friction to the lander body. The attitude stability of Philae, a prerequisite also for the rather stable RF link, is also due to that angular momentum. After TD1, just before the collision, Philae rotated with about 0.075 Hz (period 13 s), after the collision with ~0.04 Hz.

Analysis of the lander footprints

We analyzed the footprint surface features seen at the TD1 site by OSIRIS NAC and NAVCAM

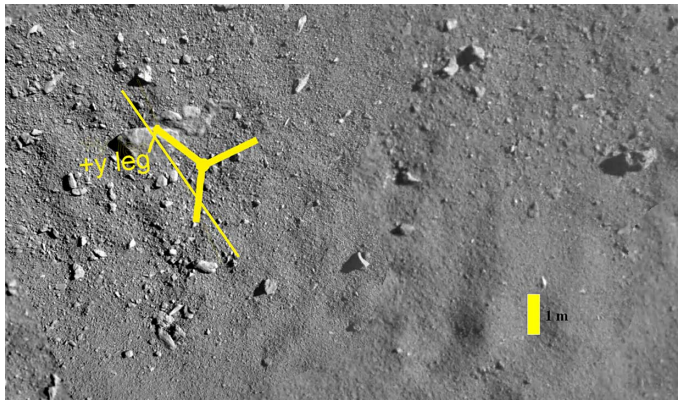

Fig. 4. Extrapolated lander position and orientation at TD1, site Agilkia. The lander legs are to scale and superimposed on merged and rectified ROLIS images. North is up. The thin yellow line indicates the –X ("balcony") side. Positional accuracy ±20 cm, yaw rotation accuracy ±1°. Philae is arriving mainly vertical, but with a lateral velocity component to the south; Philae rotates by ~0.67°/s counterclockwise (top view) about its *z* axis, ~12 ± 1° inclined to the local surface normal.

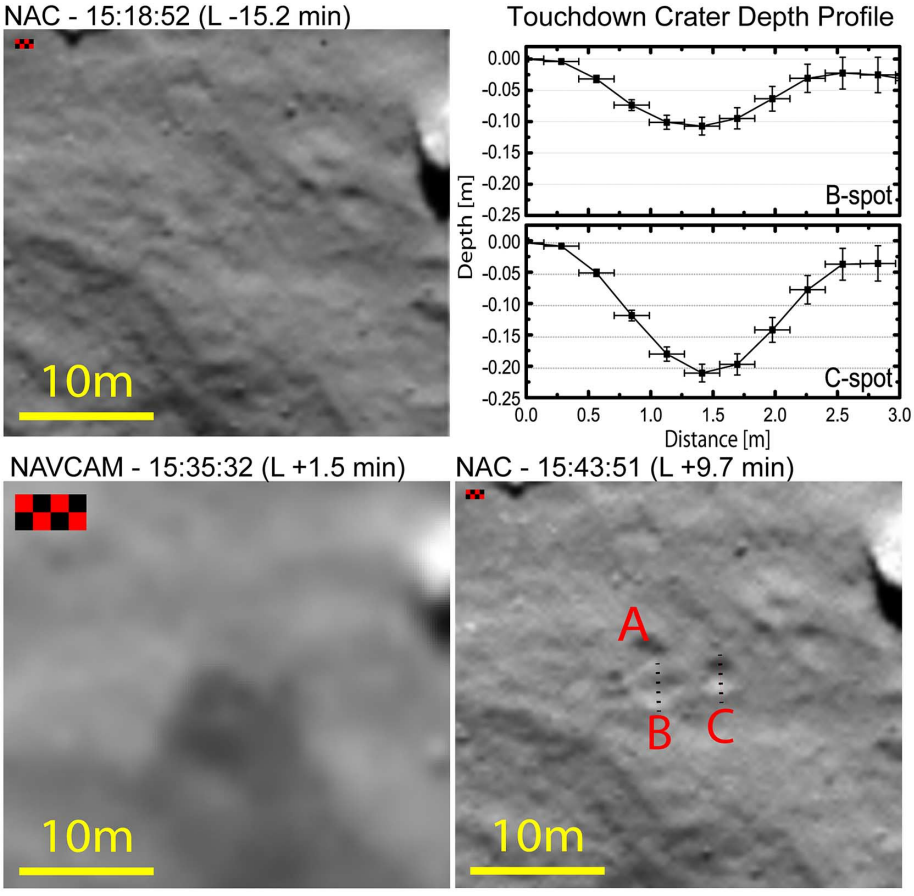

Fig. 5. Surface morphology changes at TD1 and associated depth profiles. Rosetta orbiter imaging of the Philae landing site: (top left) OSIRIS NAC image from landing (L) –15.2 min (0.29 m/pixel); (bottom left) NAVCAM image from L + 1.5 min (1.30 m/pixel); (bottom right) OSIRIS NAC image from L + 9.7 min (0.28 m/pixel). The top right shows the depth profile through the B spot and C spot, respectively. The images were acquired from a distance of ~15.2 km (*12*). The black and red checkerboard bars indicate the pixel size.

images (Fig. 5 and figs. S12 to S15). It is not fully understood yet which feature was caused by which structural part of the lander and in which sequence; however, it appears almost certain that two of the new features are depressions, some 0.1 and 0.2 m deep and 2 m in diameter (Fig. 5, features B and C). Feature A, apparently, is not a depression, because there is no change in reflectance as we see it in the two other features: A is probably the projection of the dust cloud (and/or its shadow) stirred up by the impact. Alternatively, A could also be "fallback" material: The NAC image was taken at TD1 + 10 min, at which time one would expect most of the material in the dust cloud to have moved away.

We used an unconstrained "shape from shading" with a generic comet surface photometric parameter set (*18*). The sensitivity of slopes and thus depth is low to Hapke parameter changes, because the angles are far away from the opposition peak of the photometric function (a full stereo photoclinometry would use multiple illumination conditions to constrain this function). We estimate the relative height uncertainties to be 10 to 20%. The horizontal accuracy is given by the image resolution (28 cm/pixel), resulting in a tentative 3σ error estimate of ~56 cm on the diameters (two pixels).

Assuming the known nucleus bulk density of 440 kg/m^3 (*19*), we roughly estimated the excavated volumes and masses of depressions B and C as V_B = 0.13 m^3, M_B ~60 kg, and V_C ~0.27 m^3, M_C ~120 kg. The total mass excavated is M = 180 kg.

Analysis of lander mechanics and inference of surface mechanical properties

We performed a preliminary energy balance analysis to determine the amount of mechanical energy dissipated in the soil for the TD1 event. From the impact kinetic energy of 49.5 J, a fraction of 5.0 J remained with the lander after TD1, where the velocity was reduced from 1 to 0.32 m/s. Friction and damping inside the lander were estimated to be 5 to 21 J during TD1. An amount of 23 to 39 J of the impact energy was transferred to the ground (*12*). Thus, the comet surface is strongly damping: 50 to 80% of the lander's kinetic energy before TD1 was dissipated in the comet soil, 10 to 40% in the damping element; and 10% was not dissipated but went into kinetic and some rotational energy after TD1.

In relation to the excavated masses (a total of depressions B and C), the energy dissipated at TD1 can theoretically accelerate all the particles up to 50 to 66 cm/s or lift them vertically up to 800 to 1400 m (gravity = 0.16 mm/s^2). These are upper limits with the assumption that no kinetic energy is transformed into heat and that there is no work against cohesion. This shows that in principle, high ejecta plumes can be formed or regolith can easily be displaced over long distances.

During Philae's FSS, several mechanical actuations were executed. A sampling by the Sampling, Drilling and Distribution Subsystem (SD2) instrument was attempted, the MUPUS-PEN (Penetrator) was deployed (*20*), and in the last moment, a translation rotation of the landing gear [a lifting by 46.3 mm and a rotation of the main body with the SG of 22.7° ± 2.5° (clockwise in top view, compare fig. S20)] was executed. In the first two cases, no major change in attitude was registered after the actuations.

The penetration of the MUPUS-PEN probe into the Abydos surface did not succeed, despite

3 hours of hammering at increasing energy levels. From this observation, the MUPUS team concludes that the crushing strength of the surface material is higher than 4 MPa (*20*).

The lander's feet carry so-called ice screws, passive elements that move out, relative to the feet soles, if a sufficient force acts on either one or both soles and the surface roughness or surface material strength permits. They can be extruded up to 70 mm if both soles are pressed up (by 70 mm) and up to 22 mm if only one sole moves (by 44 mm). At Abydos, only one ice screw (that of the +X foot) can be confirmed (*21*) to have moved (the right sole seen from the center ~50 mm up); on the +Y foot, possibly the left sole has moved ≤10 mm up. The –Y foot cannot be analyzed because of lack of illumination. We do not know at which surface contact this ice screw was activated, but suspect TD1. Because the ice screws have an internal reverse lock, they remain extended after first activation. The lander's feet and ice screws hardly, if at all, penetrated the surface at Abydos. This can be seen in CIVA (Comet Infrared and Visible Analyser) panoramic images showing the feet (*21*), supporting the idea that the surface at Abydos is much harder than at Agilkia.

Discussion

Because the mechanical response of Philae (damping element, structural elasticity, rotation, and flywheel) is complicated and superimposed on the surface strength decelerations upon touchdown, we combined a soil mechanics force model (*3*, *11*) with a numerical multibody simulation of Philae (*10*) that was calibrated and verified with test data from a Philae mockup (*10*, *22*). The goal is to determine the soil properties, including strength, elastic constants, dissipation, excavation mechanics, possible layering, and horizontal inhomogeneity (e.g., boulder versus finer regolith).

We performed a first parameter study using the above multibody lander model and assumed a simple soil model: homogeneous regolith characterized only by its uniaxial compressive strength C set equal to the constant penetration resistance; i.e., the material can be displaced to the sides. The results obtained by varying only C indicate that foot-sole penetrations were in the range of a few centimeters for C ~ 10 kPa and below. Compressive strength values much exceeding 10 kPa reduce the footpad penetration to millimeters. The rebound velocity is reproduced to ±20% in magnitude but not yet its direction. All these values are to be taken with caution, because they are sensitive to the transversal velocity component, due to less-effective damping, additional sliding friction, the induced angular momentum, and the inhomogeneity of the soil.

From Fig. 4, it is intriguing to imagine that for the first contact, the +Y foot just hit an approximately 1-m sized "boulder." However, there is still a ~0.2-m uncertainty in the foot position at first contact relative to the terrain, so the +Y foot might just have missed the edge of that boulder. Also, the horizontal component of the impact velocity could have led to a sliding motion on the boulder, or the impact on a boulder is mechanically not very different from that on finer regolith. We do not exclude the possibility that the SESAME-CASSE data can be explained by either scenario.

We discuss an alternative interpretation of SESAME-CASSE data at TD1. Here, it is assumed that the first signal seen on the +Y foot (at 15:34:03.98) corresponds to the first contact with a soft layer, and the beginning of the strong signal ~0.27 s later to impact on a stiff and hard surface. With the initial normal velocity of the foot (1 m/s), the soft layer then has a maximum thickness of 0.25 m and less if the foot was noticeably decelerated by this layer (which is not supported by the CASSE accelerometer data). This would be consistent with the depth profile of the lander footprint features. For the estimated thickness of the upper soft layer of 0.1 to 0.2 m, a conservative upper limit for the compressive strength C_{max} of that layer, if assumed homogeneous, can be estimated: Neglecting the (slower) damping mechanism, penetrating a homogenous layer with compressive strength C, by a mass M, initial velocity v_0, frontal area A gives a maximum depth $y_e = Mv_0^2/(2CA)$. With the reduced mass (*12*) M = 17.4 kg, v_0 = 1.01 m/s, $A = 0.017n$ m^2 (n = 2: the number of feet penetrating almost simultaneously), C_{max} = 1 to 3 kPa. The postulated competent layer below has an unknown thickness, with an unknown compressive strength. Only its elastic parameters can be estimated from the CASSE signals using Hertz's contact theory and the sole's resonances (*22*). Yet this layer appears to be strong and/or thick enough to withstand the dynamical loads exerted by Philae's feet, because breakage of that layer and transition to the presumably soft granular material beneath is not seen in the data. The minimum thickness of the assumed hard layer to withstand landing without failure can be estimated to be on the order of 0.3 to 3 cm, using realistic parameters (*12*).

The tentative mechanical model of the upper surface layers is as follows: At Agilkia, there is a granular soft surface consisting of regolith with a depth of at least ~20 cm and typical ≤1-cm particle sizes with a compressive strength on the order of 1 kPa, and at Abydos (and probably also at the COL (collision with crater rim) and TD2 sites, there is a hard and stiff surface with a (crushing) strength of at least 2 MPa. This layer may be similar to the possible subsurface "competent" layer at Agilkia. The unexpectedly high strength of the hard material is similar to that of the "sintered layer" found in the Kometensimulation (KOSI) laboratory experiments on insolated cometary analog materials in vacuum (*1*), suggesting that the cometary matter near the surface may be processed and thus not representative of the pristine state after formation.

The two sites Agilkia and Abydos are situated in two different morphological regions: very likely in Ma'at and Bastet. Whereas the Ma'at region appears to be covered by a smooth "dust" layer (*15*, *23*) with a brittle underlayer, Bastet is described as an exposed consolidated surface with minimal bouldering, possibly part of the basal unit. The size distribution of the regolith at Ma'at is now constrained by ROLIS data as still granular at 0.9 cm/pixel and is interpreted as "airfall" (*15*). Both morphological descriptions are consistent with our observations.

The tensile strength of some overhangs on 67P has been previously estimated at between 10 and 200 Pa (*15*). We believe that this represents a lower bound, because the overhangs still exist (although debris is seen at the lower edges). The breaking stresses at the rim of the overhang are caused by gravity. If there are any cavities or crack-like features in the overhangs, they act as a stress concentrator, and that would explain the variability. These low values for the (minimum) tensile strength on large scales do not contradict the findings as reported here; they are not even comparable: We measure compressive strength here on 0.1–to–1-m scales, whereas the estimate in (*15*) refers to tensile (or shear) strength on >10-m scales. Compressive strength can be orders of magnitude higher than tensile strength in a granular material (*3*, *24*).

Although previous ex situ determinations of the strength of cometary matter (*5*, *6*) are consistent with our conclusions, it is important to note that the values of strength on scales on the order of ~10 cm (the diameter of the lander feet) or meters (the lander body) on the surface of an active comet follow different physical processes, including the interaction of individual grains, sintering processes, the presence of cracks and pores, or the formation of a crust layer. In particular, the formation of a crust layer, at places overlaid with airfall regolith, also explains differences in strength of a cometary surface as compared to the bulk regolith properties [e.g., as modeled in (*2*)].

REFERENCES AND NOTES

1. H. Thomas, L. Ratke, H. Kochan, Crushing strength of porous ice-mineral bodies-relevance for comets. *Adv. Space Res.* **14**, 207–216 (1994). doi: 10.1016/0273-1177(94)90271-2; pmid: 11539952
2. J. Blum, B. Gundlach, S. Mühle, J. M. Trigo-Rodriguez, Comets formed in solar-nebula instabilities! - An experimental and modeling attempt to relate the activity of comets to their formation process. *Icarus* **235**, 156–169 (2014); correction: *Icarus* **248**, 135–136 (2015). doi: 10.1016/j.icarus.2014.03.016
3. J. Biele *et al*., The putative mechanical strength of comet surface material applied to landing on a comet. *Acta Astronaut.* **65**, 1168–1178 (2009). doi: 10.1016/j.actaastro.2009.03.041
4. K. A. Holsapple, K. R. Housen, in *Proceedings of the 37th LPSC, XXXVII*, League City, TX, 13 to 17 March 2006, no. 1068.
5. J. M. Trigo-Rodríguez, J. Llorca, The strength of cometary meteoroids: Clues to the structure and evolution of comets. *Mon. Not. R. Astron. Soc.* **372**, 655–660 (2006); erratum: *Mon. Not. R. Astron. Soc.* **375**, 415–415 (2007). doi: 10.1126/science.1135840; pmid: 17170289
6. D. Brownlee *et al*., Comet 81P/Wild 2 under a microscope. *Science* **314**, 1711–1716 (2006). doi: 10.1126/science.1135840; pmid: 17170289
7. M. F. A'Hearn *et al*., Deep Impact: Excavating comet Tempel 1. *Science* **310**, 258–264 (2005). doi: 10.1126/science.1118923; pmid: 16150978
8. W. Kofman *et al*., Properties of the 67P/Churyumov-Gerasimenko interior revealed by CONSERT radar. *Science* **349**, aab0639 (2015).
9. S. Hegler *et al*., Operation of CONSERT aboard Rosetta during the descent of Philae. *Planet. Space Sci.* **89**, 151–158 (2013). doi: 10.1016/j.pss.2013.09.015
10. L. Witte *et al*., Experimental investigations of the comet Lander Philae touchdown dynamics. *J. Spacecr. Rockets* **51**, 1885–1894 (2014). doi: 10.2514/1.A32906

11. N. Kömle *et al.*, Impact penetrometry on a comet nucleus-interpretation of laboratory data using penetration models. *Planet. Space Sci.* **49**, 575–598 (2001). doi: 10.1016/S0032-0633(00)00169-0
12. Complete materials and methods are available as supplementary materials on *Science* Online.
13. E. Heggy *et al.*, Radar properties of comets: Parametric dielectric modeling of Comet 67P/Churyumov-Gerasimenko. *Icarus* **221**, 925–939 (2012).
14. P. Kamoun, P. L. Lamy, I. Toth, A. Herique, Constraints on the subsurface structure and density of the nucleus of Comet 67P/Churyumov–Gerasimenko from ARECIBO radar observations. *Astron. Astrophys.* **568**, A21 (2014). doi: 10.1051/0004-6361/201423544
15. N. Thomas *et al.*, The morphological diversity of comet 67P/Churyumov-Gerasimenko. *Science* **347**, aaa0440 (2015). pmid: 25613893
16. ESA's Planetary Science Archive, www.rssd.esa.int/index.php?project=PSA&page=rosetta.
17. H.-U. Auster *et al.*, The nonmagnetic nucleus of comet 67P/Churyumov-Gerasimenko. *Science* **349**, aaa5102 (2015).
18. S. Fornasier *et al.*, Spectro-photometric properties of the 67P/Churyumov-Gerasimenko's nucleus from the OSIRIS instrument onboard the ROSETTA spacecraft. *Astron. Astrophys.* 10.1051/0004-6361/201525901 (2015).
19. H. Sierks *et al.*, On the nucleus structure and activity of comet 67P/Churyumov-Gerasimenko. *Science* **347**, aaa1044 (2015). doi: 10.1126/science.aaa1044; pmid: 25613897
20. T. Spohn *et al.*, Thermal and mechanical properties of the near-surface layers of comet 67P/Churyumov-Gerasimenko. *Science* **349**, aab0464 (2015).
21. J.-P. Bibring *et al.*, 67P/Churyumov-Gerasimenko surface properties as derived from CIVA panoramic images. *Science* **349**, aab0671 (2015).
22. C. Faber *et al.*, A method for inverting the touchdown shock of the Philae Lander on Comet 67P/Churyumov-Gerasimenko. *Planet. Space Sci.* **106**, 46–55 (2015). doi: 10.1016/j.pss.2014.11.023
23. S. Mottola *et al.*, The structure of the regolith on 67P/Churyumov-Gerasimenko from ROLIS descent imaging. *Science* **349**, aab0232 (2015).
24. J. Tomas, Fundamentals of cohesive powder consolidation and flow. *Granul. Matter* **6**, 75–86 (2004). doi: 10.1007/s10035-004-0167-9

ACKNOWLEDGMENTS

Rosetta is an ESA mission with contributions from its member states and NASA. Rosetta's Philae lander is provided by a consortium led by DLR, MPS, CNES, and Agenzia Spaziale Italiana (ASI). Further important contributions came from the Magyar Tudományos Akadémia Wigner Fizikai Kutatóközpont, Max-Planck-Institut für Extraterrestrische Physik (MPE), the Finnish Meteorological Institute (FMI), the UK Space Agency, Space Technology Ireland Ltd. (STIL), and IWF. The contribution of the ROMAP and RPC-MAG [Rosetta Plasma Consortium (RPC) Fluxgate Magnetometer] team was financially supported by the German Ministerium für Wirtschaft und Energie and the Deutsches Zentrum für Luft- und Raumfahrt under contract 50QP1401. The contribution of the CONSERT team was supported by CNES, CNRS, and Université Joseph Fourier, Grenoble. The images and data used in this study are archived in (*16*). The authors thank the teams of Rosetta and Philae, including those for the scientific instruments, for making this endeavor possible. Special thanks go to the ESA flight dynamics team for its strong support to prepare and realize the landing of Philae. This mission would not have been possible without the outstanding contributions of the orbiter instrument teams needed for landing site selection and lander operations, in particular the OSIRIS, MIRO (Microwave Instrument for the Rosetta Orbiter), VIRTIS (Visible, Infrared, and Thermal Imaging Spectrometer); ALICE (An ultraviolet imaging spectrometer for the Rosetta orbiter), and ROSINA (Rosetta Orbiter Spectrometer for Ion and Neutral Analysis) teams. Special thanks go to M. Hilchenbach for stimulating discussions and M. Hofmann, P. Gutiérrez-Marqués, and C. Tubiana for the processing of OSIRIS images for this paper. The authors also express their appreciation to H. Rosenbauer, whose effort and inspiration were essential ALICE (An ultraviolet imaging spectrometer for the Rosetta orbiter)for the realization of Philae.

SUPPLEMENTARY MATERIALS

www.sciencemag.org/content/349/6247/aaa9816/suppl/DC1
Materials and Methods
Supplementary Text
Figs. S1 to S20
Tables S1 to S6
Movie S1

23 February 2015; accepted 26 June 2015
10.1126/science.aaa9816

The landing(s) of Philae and inferences about comet surface mechanical properties

Jens Biele, Stephan Ulamec, Michael Maibaum, Reinhard Roll, Lars Witte, Eric Jurado, Pablo Muñoz, Walter Arnold, Hans-Ulrich Auster, Carlos Casas, Claudia Faber, Cinzia Fantinati, Felix Finke, Hans-Herbert Fischer, Koen Geurts, Carsten Güttler, Philip Heinisch, Alain Herique, Stubbe Hviid, Günter Kargl, Martin Knapmeyer, Jörg Knollenberg, Wlodek Kofman, Norbert Kömle, Ekkehard Kührt, Valentina Lommatsch, Stefano Mottola, Ramon Pardo de Santayana, Emile Remetean, Frank Scholten, Klaus J. Seidensticker, Holger Sierks and Tilman Spohn

Science **349** (6247), aaa9816.
DOI: 10.1126/science.aaa9816